ELSEVIER

Journal of Nuclear Materials 295 (2001) 265–272

journal of nuclear materials

www.elsevier.nl/locate/jnucmat

Radiation resistance and thermal creep of ODS ferritic steels

V.V. Sagaradze [a,*], V.I. Shalaev [a], V.L. Arbuzov [a], B.N. Goshchitskii [a], Yun Tian [b], Wan Qun [c], Sun Jiguang [c]

[a] *Institute of Metal Physics, Ural Branch RAS, 18 S. Kovalevskaya Str., Ekaterinburg 620219, Russia*
[b] *Central Iron and Steel Research Institute, Beijing, People's Republic of China*
[c] *General Research Institute for Non-ferrous Metals, Beijing 100088, People's Republic of China*

Received 6 June 2000; accepted 22 February 2001

Abstract

Oxide dispersion strengthened (ODS) ferritic steels containing 0.38–0.39 wt% Y_2O_3 have been produced by mechanical alloying. After thermo-mechanical treatment, the structure of ODS steels includes polygonized extended grains and a great number (to $\sim 10^{16}$–10^{17} cm^{-3}) of ultrafine complex yttrium oxides ~2–3 nm in diameter. Irradiation by fast neutrons to 4.5×10^{26} n/m^2 (340 K) and 1.5×10^{22} n/m^2 (77 K) leads to strengthening and plasticity decreasing in ODS alloys. The advantages of ODS ferritic steels in creep resistance and strength against ferritic-martensitic steel 12Cr–2Mo–Nb–B–V and austenitic steel 16Cr–15Ni–3Mo–Ti–V display obviously when creep rate is approximately 10^{-2} h^{-1} and fracture time is longer than 1000 h.

1. Introduction

Oxide dispersion strengthened (ODS) ferritic steels possess not only excellent resistance to neutron irradiation-induced swelling but also to high-temperature creep, so they are believed to be most promising candidate materials for cladding of advanced fast reactors and are studied extensively [1–6]. Excellent creep resistance of the alloys is due to ultrafine oxide articles (Y_2O_3 or $Y_2Ti_2O_7$), which are stable at high temperatures [3,4, pp. 65–82]. Some investigations showed that these dispersed oxide particles not only impart superior creep properties to steels, but also improve neutron swelling resistance. Moreover, ODS ferritic steels with bcc structure possess ability to suppress void swelling better than the austenitic stainless steels with fcc structure. For example, the ODS alloy Fe–14Cr–1Ti–$0.3Y_2O_3$ irradiated with 4-MeV Ni ions up to 150 dpa at 723 and 923 K had no swelling ($\Delta V/V < 0.1\%$) [6]. However, some major issues remain unclear: (1) how would mechanical properties of the alloy change under neutron irradiation at different temperatures? (2) Which are the main advantages of the alloy over austenitic and ferritic–martensitic steels used as reactor materials? This study deals with these issues.

2. Materials and experimental technique

The chemical composition of the ODS steels under study is given in Table 1.

Test samples were prepared as follows. Fe, Cr, W or, Cr–Fe–Ti and Y_2O_3 (~0.39 wt%) powders were mechanically alloyed and then were placed in a container. The mixture was outgassed and hot-pressed at 1373 K to form rods 30 mm in diameter. The steels under study differ not only by their composition, but also by conditions of mechanical alloying. Starting powders of the K2 steel were ground in ball mills for 36 h. The mass ratio of the balls and the powder was 10:1. The average speed of the balls was 110 rpm. Starting powders of K5 and K7 steels were ground in mills for 48 h. The mass ratio of the balls and the powder was 15:1. The average speed of the balls was 150 rpm.

* Corresponding author. Tel.: +7-3432 744 214; fax: +7-3432 740 003.
E-mail addresses: rdnr@neutron.e-burg.su, vsagaradze@imp.uran.ru (V.V. Sagaradze).

0022-3115/01/$ - see front matter
PII: S0022-3115(01)00511-6

Table 1
Chemical composition (wt%) of ODS ferritic steels

ODS-steels	Cr	Ti	Mo	Y_2O_3	W	Al	O	N	C
K2	13.08	2.23	1.43	0.38	–	–	0.54	0.16	0.02
K5	13.51	1.32	0.6	0.39	–	0.17	0.24	0.015	0.011
K7	13.44	1.14	0.19	0.39	2.11	0.16	0.24	0.022	0.007

The K2 alloy was irradiated with fast neutrons in a BOR-60 reactor at the irradiation temperature of 683 K and the fluence of 4.5×10^{26} n/m^2 (damaging dose being 20 dpa). Tensile flat samples were 1×4 mm^2 in cross-section and had the working zone 11 mm long. Tensile experiments were performed at 293, 523, 673 and 823 K after irradiation. To determine proneness of the steels to embrittlement under neutron irradiation, samples were exposed to low-dose neutron irradiation (fluence of 1.5×10^{22} n/m^2) in an IVV-2 M reactor at 77 K. Irra-

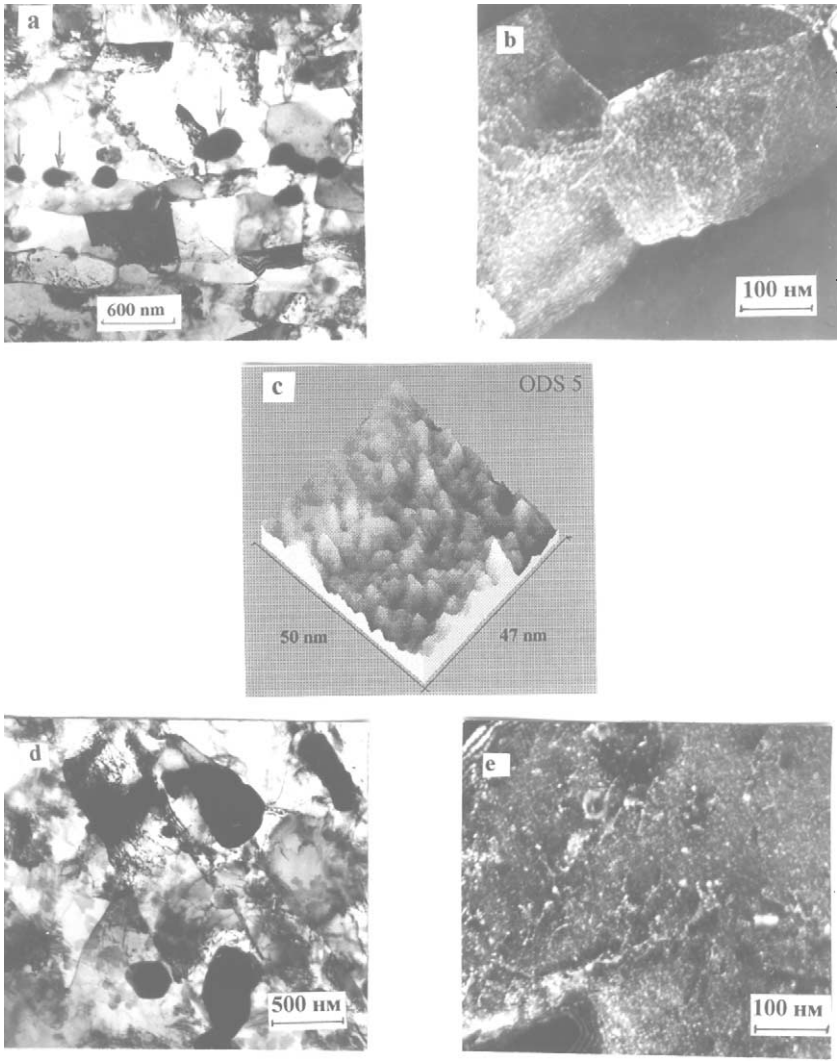

Fig. 1. Structure of the ODS steels types K7 (a,b,d,e) and K5 (c) with ~0.39 wt% Y_2O_3 after mechanical alloying in a ball mill, outgassing in a container, and sintering during hot deformation and annealing at 1373 K: (a) polygonal structure and coarse particles (shown with arrows); (b) dark-field TEM image of fine ittrium-titanium oxides; (c) ultrafine oxides in a scanning tunnel microscope; (d,e) particles after creep (923 K, $\sigma = 350$ MPa, $\tau = 4292$ h).

diated tensile samples were tested at 77, 293, 523, 673 and 833 K. The microstructure was examined in a JEM-200CX electron microscope. Annealing of point defects during low-temperature irradiation was measured and analyzed by the resistometric method. The samples were annealed isochronally (25 min) every 25–50 K from 77 K at a rate of 1 K/min. Electroresistance of annealed samples was measured to within 0.05% at the liquid nitrogen temperature.

In order to study pore volume during mechanical alloying of ODS-steels the effect of the implantation dose F on accumulation of implanted hydrogen in radiation-damaged areas of the ODS steels was analyzed by the nuclear reaction method using the D(d,p)T reaction, which yields tritium and protons. The samples were irradiated with 700-keV deuterons and the concentration of implanted deuterium was measured simultaneously at room temperature. The radiation-damaged zone and the implantation and measurement zones coincided (0–4 μm). The deuterium concentration was determined using the TRIM program and a reference sample of $TiD_{1.78}$ with a uniform distribution of deuterium C^D. The C^D distribution was measured with an accuracy of ~5% of the measured value.

Creep samples were cut from plates in the form of dumb-bells and were strengthened with stainless steel plates. A pin hole was drilled in each 'bell'. The working zone of the samples was about $1 \times 4 \times 11$ mm^3 for K2 and about $1 \times 4 \times 18$ mm^3 for K5 and K7. Creep tests were performed on a standard machine type AIMA-5-3 at temperatures from 923 to 973 K under a constant load. The load was maintained automatically to within one percent. The temperature was kept constant with the same accuracy. The test stress interval was 150–450 MPa. For the sake of comparison, properties of the 16Cr–15Ni–3Mo–Ti–V and 16Cr–15Ni–3Mo–1Ti austenitic steel and the 12Cr–2Mo–Nb–B–V ferritic-martensitic steel used in reactor applications were measured.

3. Results and discussion

3.1. Mechanical properties of the ODS ferritic steels irradiated with fast neutrons at 683 K up to 20 dpa

Fig. 1 shows the initial structure of the ODS ferritic steels prior to irradiation. It is clearly seen that the steel grains extend along the working direction. The alloy structure is polygonized (non-recrystallized). The grains are 1–3 μm long and 250–500 nm wide. Titanium carbonitride and χ-phase [3] (150–200 nm in size) are located mostly at grain and subgrain boundaries (Fig. 1(a)). The ODS steels K5 and K7 treatment provided a better grinding quality and better deformation dissolution of yttrium oxides having the average initial size of 30 nm. As a result, much more ultrafine (nanosized) complex oxides $Y_2O_3xTiO_2$ (Y_2TiO_5) [3,4, pp. 65–82] precipitate in K5 and K7 ODS steels than in the K2 ODS steel (Figs. 1(b) and (c)) during sintering and final thermal treatment (quenching from 1373 K in air). The number density of the oxide particles in K2, K5, K7 steels is 4×10^{16}, 2×10^{17}, and 1.6×10^{17} cm^{-3}, respectively. Maximum oxide size is ~3.3 nm (K7 steel). These particles pin dislocations, do not dissolve during heating, and prevent recrystallization even at 1373 K. Clearly, at 293 K the yield stress $\sigma_{0.2}$ of the K2 steel (where the number of Y_2TiO_5 particles is much less than in K5) will be ~350 MPa lower than that of the K5 steel (see Table 2). The K7 steel, which contains ~2 mass% W as compared to 0.6 mass% Mo in the K5 steel, has a maximum short-time strength at 923 K (Table 2). Let it be noted that such high properties cannot be imparted to the ODS steels in the initial (quenched) state by the method of high-temperature sintering (without preliminary optimal mechanical alloying), because coarse starting oxides will not dissolve and, consequently, ultrafine oxides ~2–3 nm in size will not precipitate.

Pores are very few and can hardly be seen by TEM in the structure of the ODS steels. Fig. 2 presents the deuterium concentration C^D as a function of the irradiation dose F. The $C^D(F)$ value increases insignificantly

Table 2
Tensile properties of ODS alloys types K2, K5 and K7 prior to irradiation

Steel	T_{test} (K)	σ_B (MPa)	$\sigma_{0.2}$ (MPa)	δ (%)
K2	293	1125	925	17.4
	923	407	–	28.6
K5	293	1360	1272	14.8
	923	525	490	27.3
K7	923	547	515	22.8

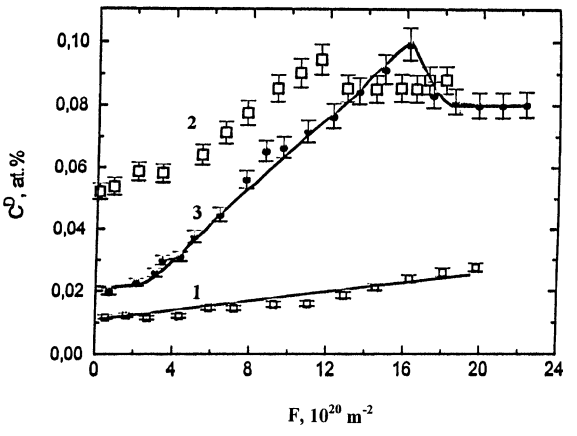

Fig. 2. Accumulation of deuterium in a smelted bcc steel with 19 at.% Cr (1) and mechanically alloyed 12Cr–2Mo–Nb–V steels (K5) with 0.39% Y_2O_3 (2) and without Y_2O_3 (3) after deuteron irradiation.

in a monotonic manner for the smelted Fe–19Cr alloy (curve 1). This dependence does not tend to saturation up to an implantation dose of $\sim 20 \times 10^{16}$ cm^{-2}. The irradiated zone of the pore-free Fe–19% Cr alloy contains much deuterium (~0.2–0.3 at.%) both in the solid solution and in the vacancy traps formed under deuterium irradiation. At implantation doses up to 25×10^{20} m^{-2} deuterium is trapped in the damaged zone more intensively in mechanically synthesized sintered ODS-1 (without yttrium oxides) and K5-ODS5 (with 0.39% Y_2O_3) steels than in the non-sintered sample Fe–19Cr. A higher concentration of deuterium accumulated at the beginning of implantation in the ODS alloys as compared to the non-sintered material is probably due to a special type of deuterium traps formed in the mechanically synthesized sintered ODS alloys. This observation can be attributed to additional deuterium traps (in the form of a small number of pores) present in mechanically alloyed ODS steels. Yttrium oxides and their interfaces are not effective deuterium traps. This conclusion is confirmed by a nearly equal amount of implanted deuterium present in the synthesized samples with and without yttrium oxides (see curves 2 and 3 in Fig. 2). If it is assumed that under the given irradiation conditions about 0.02–0.03 at.% deuterium (see the curve 1 in Fig. 2) dissolves in the pore-free Fe–Cr matrix, then voids in ODS steels should accumulate about 0.07–0.08 at.% deuterium (see the upper curves 2–3 in Fig. 2). Usually the void gas has a high pressure. If the deuterium void pressure is taken to be $\sim 0.1\sigma_{0.2}$ ~100 MPa pore volume should be ~0.16 vol.%.

The ODS ferritic alloys possess excellent strength and adequate plasticity at 293 and 923 K before irradiation (Table 2).

After neutron irradiation (4.5×10^{26} n/m^2, ~20 dpa, 683 K) tensile strength of the ODS alloys increases insignificantly (the yield stress $\sigma_{0.2}$ and the ultimate strength σ_B of K2 at 20°C are 1290 and 1465 MPa, respectively), but their plasticity is impaired (elongation δ decreases to 1.1%) – Table 3. The steels show a clear-cut tendency to brittleness. Their plasticity is comparable with plasticity of conventional ferritic and ferritic-martensitic bcc steels after fast-neutron irradiation. The fcc stainless steel 16Cr–15Ni–3Mo–1Ti (steel 66) preserves its plasticity even when exposed to a high dose of fast-neutron irradiation (60 dpa), see Table 3. When the test temperature is elevated from 293 to 823 K, the tensile strength of the ODS ferritic alloy decreases slightly, but elongation δ is not recovered and remains very small. Plasticity of the irradiated 16Cr–15Ni–3Mo–1Ti fcc steel is very low ($\delta = 2.3\%$) at 823 K and is comparable with plasticity of the ODS ferritic alloy. Strengthening and the corresponding embrittlement of the ODS ferritic alloys after fast-neutron irradiation (Table 3) can be explained by formation of dislocation loops and radiation-induced precipitation of particles, probably, of titanium nitride or carbonitride. A high concentration of nitrogen and carbon (C + N = 0.18 wt%) in the K2 alloy may be conducive to this effect. Moreover, neutron irradiation of bcc alloys containing over 12% of ferrite-forming elements Cr, Mo and Ti can lead to partial precipitation of the α'-phase at 673–748 K [7,8]. Formation of the α'-phase causes strengthening and the so-called 475°C embrittlement. This is probably the reason why strength characteristics are higher at $T_{test} = 400$°C than at $T_{test} = 250$°C (see Table 3). The Cr concentration of ferritic and ferritic-martensitic steels was recently limited to 9 wt% to avoid embrittlement [9]. Probably, plasticity of K5 and K7 alloys would decrease to a lesser extent under irradiation thanks to low concentrations of nitrogen, carbon and oxygen.

Table 3
Tensile properties of the K2 alloy and the 66 steel (16Cr–15Ni–3Mo–1Ti) irradiated with fast neutrons to 20 and 60 dpa at 683 and 753 K, respectively

Steel	T_{test} (K)	σ_B (MPa)	$\sigma_{0.2}$ (MPa)	δ (%)
K2 ($T_{irr} = 683$ K, 20 dpa)	293	1465	1290	1.1
	523	1155	1110	1.0
	673	1270	1170	0.95
	823	980	900	1.25
66 ($T_{irr} = 753$ K, 60 dpa)	293	942	807	14.9
	823	718	663	2.3

3.2. Mechanical properties of the ODS ferritic steels after low-temperature neutron irradiation at a fluence of 1.5×10^{22} n/m^2

To determine the propensity of the ODS ferritic alloys to embrittlement under exposure to small fluences, the alloys were neutron-irradiated at 77 K. At this temperature, radiation-induced vacancies and interstitials are virtually immobile and accumulate mainly in low-temperature displacement cascades. It was shown [10] that a small neutron fluence of 1.5×10^{22}–15×10^{22} n/m^2 also causes brittleness of bcc materials (for example, Fe–13Cr, V–10Ni–5Cr, or V–4Ni–4Cr) under similar conditions (Fig. 3). Table 4 presents mechanical properties of the K5 ODS steel and the conventional Fe–13Cr ferritic alloy (which is the basis of many ferritic, martensitic, and ferritic-martensitic steels used in reactor applications) at 77 K after low-temperature irradiation (fluence of 1.5×10^{22} n/m^2). After irradiation at 77 K, the ODS alloy was completely brittle ($\delta = 0\%$). The samples failed in the elastic range during the tests. During the intermediate annealing at 298 K vacancies and interstitial recombine or flow to sinks and slightly improved the plasticity of the ODS alloy ($\delta = 0.5\%$) at 77 K and allowed determining the strength characteris-

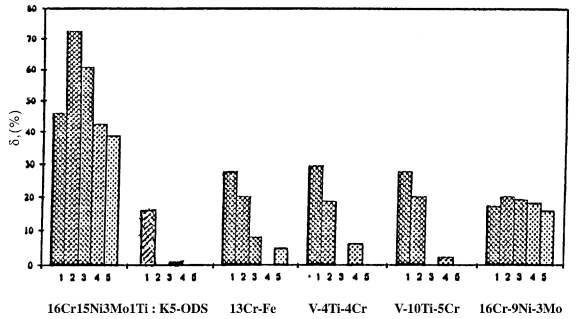

Fig. 3. Bar chart showing plasticity δ of steels and alloys irradiated at 77 K: 16Cr–15Ni–3Mo–1Ti; K5 ODS; 13Cr–Fe; V–4Ti–4Cr; V–10Ti–5Cr; 16Cr–9Ni–3Mo. Bars 1–5 give the test temperature T (K) and the neutron fluence F (n/m^2) for each alloy: (1) $T = 298$ K, $F = 0$; (2) $T = 77$ K, $F = 0$; (3) $T = 77$ K, $F = 1.5 \times 10^{22}$; (4) $T = 77$ K, $F = 7 \times 10^{22}$; (5) $T = 77$ K, $F = 15 \times 10^{22}$.

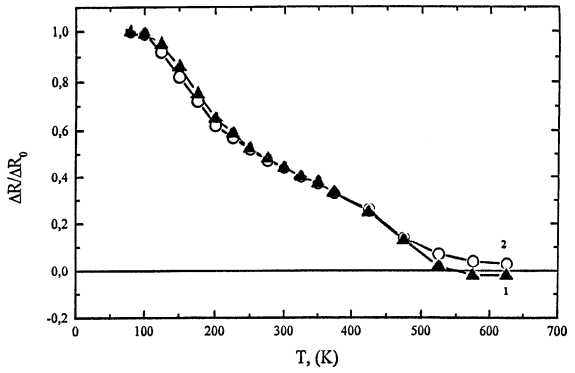

Fig. 4. Relative electroresistance $\Delta R/\Delta R_0$ (as measured at 77 K) of the Fe–19Cr alloy (1) and the K5 ODS steel versus the successive isochronal annealing temperature (0.5 h). Preliminary treatment: neutron irradiation at 77 K (fluence of 15×10^{22} n/m^2).

tics: $\sigma_{0.2} = 1835$ and $\sigma_B = 1890$ MPa (see Table 4). Plasticity changed little during tests at 298 K, but $\sigma_{0.2}$ and σ_B decreased to 1505 and 1546 MPa, respectively.

Fig. 4 shows the relative electroresistance of irradiated samples $\Delta R/\Delta R_0$ (ΔR_0 being the increment in electroresistance after irradiation) as a function of the isochronal annealing temperature. From Fig. 4 it is seen that at 298 K electroresistance of the ODS alloy and the conventional Fe–19Cr ferritic steel is recovered by 55% only. That is, not all point defects recombined or disappeared at sinks. Electroresistance is recovered completely at 523 K. Electroresistance of the K5 alloy and

Table 4
Tensile properties of Fe–13Cr, K5, and 16Cr–15Ni–3Mo–1Ti steels upon exposure to a small neutron fluence F at 77 K

Steels	$F \times 10^{22}$ (n/m^2)	Sample no	$\sigma_{0.2}$ (MPa)	σ_B (MPa)	δ_u (%)	δ (%)
Fe–13Cr Test 293 K	0	1–3	128	340	–	28
Fe–13Cr Test 77 K	0	4–6	766	846	–	20
Fe-13Cr Irr. 77 K	1.5	X–2	1035	1035	0	7.9
Test 77 K	15	X–7,8,2	1103	1103	0	4.7
Fe–13Cr Irr. 77 K + 298 K (24 h)	I5	X–3,4,9	1179	1179	0	1.8
Test 77 K						
Fe–13Cr Irr. 77 K + 473 K (24 h)	15	X–10	1215	1215	0	1.5
Test 77K						
Fe–13Cr Irr. 77 K,	15	X–5,6,11	470	480	7.2	14.4
Test 293 K						
K5–ODS Irr. 77 K,	1.5	K–1	1795	1795	0	0
Test 77 K		K–11	1715	1715	0	0
K5–ODS Irr. 77 K + 298 K (24 h),	1.5	K–8	1835	1890	0.5	0.5
Test 77 K						
K5–ODS Irr. 77 K,	1.5	K–5	1505	1546	0.7	0.7
Test 298 K						
16Cr–15Ni–3Mo–1Ti Irr. 77 K,	0	0,47,49	530	1162	65.8	72.3
Test 77 K	1.5	45,46	762	1223	56.3	60.6
	7	54,56,57	1026	1313	35.4	41.8
	15	64,66,67	1097	1320	30.7	383
16Cr–15Ni–3Mo–1Ti Irr. 77 K,	0	A3	242	610	26.4	46
Test 293 K	1.5	38,39	403	670	22.0	30.2
	7	51,58	528	728	22.0	25.8
	15	65,68	540	740	–	26.3

the conventional ferritic steel changed to the same extent upon heating (Fig. 4). Consequently, point defects exhibit a similar behavior in these steels. The possible formation of titanium carbonitrides during annealing of deuterium-irradiated ODS steels probably has little effect on the relative electroresistivity. The dependence $\Delta R/\Delta R_0 = f(T)$ exhibits a similar temperature trend for steels with (K5) and without (Cr19) titanium (see curves 1 and 2 in Fig. 4). However, mechanical properties of the Fe–Cr ferritic alloy and the ODS steels change differently. When exposed to a low-temperature neutron fluence of up to 15×10^{22} n/m^2, the conventional Fe–13Cr ferritic steel becomes extremely brittle at 77 K: the uniform elongation δ_u decreases to zero and the general elongation δ drops to 1.5–4.7%. Plasticity is not improved after intermediate annealing at 278 and 473 K. Fig. 3 shows plasticity diagrams of various candidate materials for reactors after low-temperature neutron irradiation [10]. The behavior of the ODS alloy is similar to that of the Fe–13Cr ferritic steel at 77 K. However, plasticity of the Fe–13Cr bcc steel is largely improved ($\delta = 14.4\%$), while the yield stress $\sigma_{0.2}$ decreases to 470 MPa at room temperature. The 16Cr–15Ni–3Mo–1Ti fcc steel preserves high plasticity $\delta = 38.3\%$ (Table 4) at 77 K after low-temperature neutron irradiation (fluence of 15×10^{22} n/m^2). The plasticity of the ODS ferritic alloys exposed to a small neutron fluence (1.5×10^{22} n/m^2) is impaired. High strength and poor plasticity of the ODS alloys are preserved even at 298 K, although plasticity is not zero. Probably, the concentration of carbon, nitrogen, oxygen and titanium should be kept optimal to preserve plasticity. For example, the 13.5Cr–2W–0.5Ti–0.25Y_2O_3 steel [11] and the K7 ODS alloy have similar compositions, but the titanium concentration is 0.55 and 1.1 wt%, respectively.

3.3. Creep properties of the ODS ferritic steels

Creep curves of the ODS ferritic steels are shown in Figs. 5–9. The creep curve of the K7 steel in Fig. 5 is typical of the ODS ferritic alloys studied. The strain is

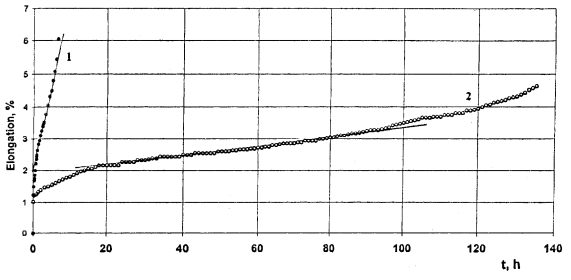

Fig. 5. Creep curves of K5 (1) and K7 (2) ODS steels at 923 K and the stress $\sigma = 400$ MPa in the 'deformation (elongation), % – time (h)' coordinates.

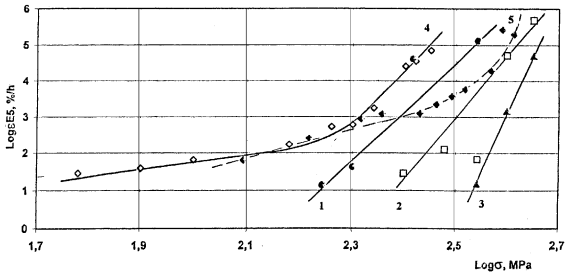

Fig. 6. The minimum creep rate ε' versus the applied stress σ at 923 K for K2 (1), K5 (2) and K7 (3) ODS steels and conventional 12Cr–2Mo–Nb–B–V bcc steel (4) and 16Cr–15Ni–3Mo–Ti–V fcc steel (5) for reactor applications.

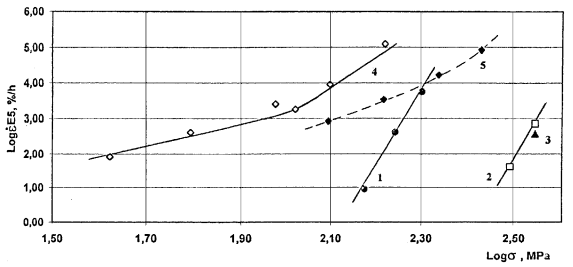

Fig. 7. The minimum creep rate ε' versus the applied stress σ at 973 K for K2 (1), K5 (2) and K7 (3) ODS steels and conventional 12Cr–2Mo–Nb–B–V bcc steel (4) and 16Cr–15Ni–3Mo–Ti–V fcc steel (5) for reactor applications.

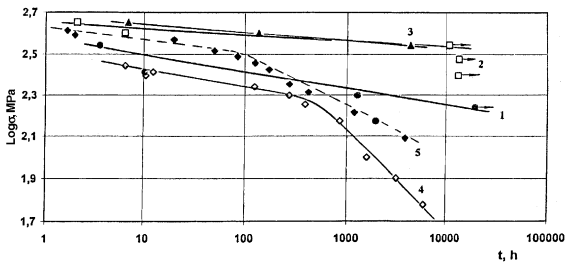

Fig. 8. Creep-rupture strength for K2 (1), K5 (2) and K7 (3) ODS steels and conventional 12Cr–2Mo–Nb–B–V (4) and 16Cr–15Ni–3Mo–Ti–V steels (5) for reactor applications.

very small at the first stage of creep, which smoothly passes to the quasi-stationary second stage, where the strain rate ε decreases slowly until the weakly pronounced third stage is reached. All broken samples of the K2 alloy had no neck and failed by intercrystallite fracture. Samples of K5 and K7 alloys failed differently. These samples had a neck when the stress σ exceeded 400 MPa. This is an evidence that the recovery process is slow, because the creep temperature of the ODS alloys is $\sim 0.5 T_{melt}$. The small recovery rate (by cross slip or climb of dislocations) suggests breaking of dislocations in the

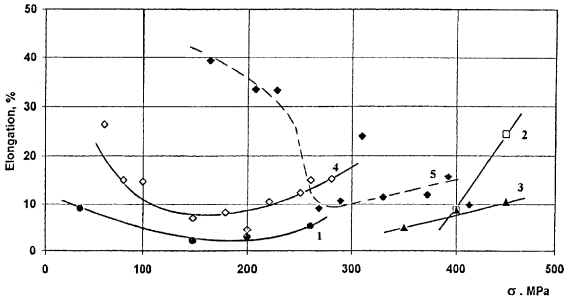

Fig. 9. Deformation (elongation, %) accumulated by the time of creep rupture depending on the applied stress σ at 923 K for K2 (1), K5 (2) and K7 (3) ODS steels and conventional 12Cr–2Mo–Nb–B–V (4) and 16Cr–15Ni–3Mo–Ti–V steels (5) for reactor applications.

ODS alloys. Simultaneously, particles of, probably, χ-phase up to 1 μm in size grow in the steels at 700°C (Fig. 4(d)). We found from experiments that the lattice constant a of the BCC χ-phase was 0.913 nm, which is 0.02 nm larger than the a of the Fe–36Cr–8Ti5Mo χ-phase determined [7] for a steel having a slightly different composition. The size (3–4 nm) of Y_2TiO_5 oxide particles changes little during creep (Fig. 4(e)) and, consequently, K5 and K7 alloys preserve their high thermal stability. The structure of the K7 alloy has the highest thermal stability, a fact which is probably due to addition of maximal volume of Y_2TiO_5 and 2.1% W.

Figs. 6–8 present experimental data relating the creep rate ε' and the time to failure τ to the applied stress σ. The $\log\varepsilon'-\log\sigma$ and $\log\tau-\log\sigma$ coordinates were chosen as the first approximation. At the working temperatures of radiation-resistant materials of fast reactors, the dependence of ε' and τ on σ for the ODS alloys in hand is given by exponential equations

$$\varepsilon' = A\sigma^{n_i} \tag{1}$$

and

$$\tau = B\sigma^{m_i}, \tag{2}$$

where A, B, n_i and m_i are constants for particular deformation conditions and σ is the initial stress calculated from the initial cross-sectional area of the sample. Exponents n_i and m_i were estimated from the curves in Figs. 6 and 7 to be between 15 and 30 for the alloys studied. It is noteworthy that these relatively high values of creep resistance persist up to $\varepsilon' \sim 10^{-4}$% per hour and $\tau \sim 10^4$ h.

The temperature dependence of the creep resistance has been so far under studied, but the apparent creep activation energy can be evaluated from the curves in Figs. 6 and 7. The creep activation energy (CAE) for the three alloys was calculated only at two temperatures. Therefore the calculation accuracy could not be determined. The CAE was about 750 kJ/mol for K2 at $\sigma = 200$ MPa, about 1050 kJ/mol for K5 at $\sigma = 400$ MPa, and about 850 kJ/mol for K7 at 350 MPa. We should be cautious about these estimates since they are very rough. Nevertheless, all the three CAE values are 2 to 3 times higher than the volume self-diffusion activation energy of bcc Fe and 1.5 to 2 times higher than the CAE of the 12Cr–2Mo–Nb–B–V reactor steel. All these results and the exponents of σ mentioned above testify to high strengthening of the ODS ferritic alloys. Obviously, strengthening is due to introduction of stable fine oxide particles in the matrix.

From the practical viewpoint, in addition to creep and fracture of the ODS alloys, it is necessary to know the limiting deformation ε_r by the moment of rupture of the ODS steels and their creep characteristics ε' and τ in comparison with those of austenitic (16Cr–15Ni–3Mo–Ti–V) and ferritic-martensitic (12Cr–2Mo–Nb–B–V) reactor steels. Fig. 9 shows the deformation ε_r of the materials after 650°C creep fracture. As is seen from this figure, ε_r values vary similarly with the stress for the K2 alloy and the 12Cr–2Mo–Nb–B–V ferritic-martensitic steel, but ε_r of the K2 steel is at least 2 times smaller than ε_r of the 12Cr–2Mo–Nb–B–V steel (ε_r of K2 does not exceed 10%). So it is inferior to ε_r of both the 12Cr–Mo–Nb–B–V steel and the 16Cr–15Ni–3Mo–Ti–V austenitic steel. The limiting deformation of K5 and K7 is not less than the maximum ε_r of K2 and approximates ε_r values of the 12Cr–Mo–Nb–B–V reactor steel.

Figs. 6 and 7 give ε' and τ as a function of the stress σ for the three ODS-steels and two (austenitic and ferritic-martensitic) reactor steels. The following conclusions can be drawn.

1. When the creep temperature is 923 and 973 K, the ODS alloys have obvious advantages over the 12Cr–2Mo–Nb–B–V bcc steel and the 16Cr–15Ni–3Mo–Ti–V fcc steel starting from the lowest steady-state creep rate $\varepsilon' \sim 10^{-2}$% per hour. When ε reaches 10^{-4}% per hour, it rises by more than three orders of magnitude for the strongest K7 alloy.
2. All the ODS alloys have better creep strength (compared to 12Cr–2Mo–Nb–B–V and 16Cr–15Ni–3Mo–Ti–V steels) starting from 200 MPa. The advantage is more pronounced when the time before failure increases to 2000 h.
3. The K2 alloy has the lowest creep resistance among all the three ODS steels studied.

4. Conclusions

1. ODS ferritic steels with 0.38–0.39 wt% Y_2O_3 (K2, K5 and K7) made by mechanical alloying have a polygonal subgrain ferritic structure, low porosity, and high strength.

2. Irradiation of the K2 steel with fast neutrons up to 20 dpa (4.5×10^{26} n/m^2) at 683 K leads to strengthening and impairment of plasticity (elongation δ is nearly 1% at 293–823 K). This is comparable with changes in plasticity of bcc steels exposed to neutron irradiation.
3. Low-temperature (77 K) neutron irradiation (fluence of 1.5×10^{22} n/m^2), which causes accumulation of low-temperature clusters in displacement cascades, leads to embrittlement of the K2 ODS steel. Plasticity is recovered to a certain extent (elongation $\delta \sim 0.5\%$) upon annealing (at 298 K) of the irradiated steels.
4. The minimum creep rate ε' and the time before failure τ as a function of the stress σ are given in the first approximation as: $\varepsilon' = A\sigma^{n_i}$ and $\tau = B\sigma^{m_i}$, where A and B are constants for particular deformation conditions, while n_i and m_i equal 15–30 and persist up to $\varepsilon' \sim 10^{-4}$ per hour and $\tau \sim 10^4$ h. The ODS ferritic steels obviously outperform the 12Cr–2Mo–Nb–B–V ferritic-martensitic and 16Cr–15Ni–3Mo–Ti–V austenitic reactor steels in creep resistance when ε' is $\sim 10^{-2}\%$ per hour and τ is longer than 1000 h. When ε' increases to $\sim 10^{-4}\%$ per hour and τ is over 2000 h, the advantage is pronounced still better. But the creep plasticity ε_r is worse than that observed for the conventional steels.

Acknowledgements

We are grateful to V.K. Shamardin, N.F. Vildanova, T.N. Kochetkova, V.D. Parkhomenko for their assistance in the experiments. This study has been supported by the Russian Fundamental Research Foundation (Project No 98-02-17341).

References

[1] J.J. Huet, Sintered Metal–Ceramic Composites, Elsevier, Amsterdam, 1984, p. 197.
[2] L. Dewilde, J. Gedopt, A. Delbrassine, C. Driesen, B. Kazimierzak, in: Proceedings of the International Conference of Materials for Nuclear Reactor Core Application, Bristol, 1987, p. 271.
[3] T. Yun, S. Bingquan, P. Qingchun et al., in: Proceeings of Materials for Advanced Energy Systems and Fission and Fusion Engineering, Southwestern Institute of Physics, Chengdu, China, 1995, p. 110.
[4] S. Ukai, M. Harada, H. Okada et al., J. Nucl. Mater. 204 (1993) 65.
[5] A.M. Wilson, M. C. Clayden, J. Standring, in: Proceedings of the International Conference of Materials for Nuclear Reactor Core Application, Bristol, 1987, p. 25.
[6] K. Asano, Y. Kohno, A. Kohyama, T. Suzuki, H. Kusanagi, J. Nucl. Mater. 155–157 (1988) 928.
[7] F.A. Garner, Nucl. Mater. Frost B.R.T.Ed. Sci. Technol. 6 (1993) 419.
[8] D.S. Gelless, Mater. Res. Soc. Symp. Proc. 373 (1995) 112.
[9] Fusion Reactor Materials VIII. Proceedings of eighth International Conference on Fusion Reactor Mater. Part B. Ferritic steels. 6.1 (1998) 1143.
[10] V.V. Sagaradze, V.L. Arbuzov, B.N. Goshchitskii, V.D. Parkhomenko, Yu.N. Zouev, V. Andryushin, Fus. Eng. Design (1998) 97.
[11] D.K. Mukhopadhyay, F.H. Froes, D.S. Gelles, J. Nucl. Mater. 258–263 (1998) 1209.